Electronic supplementary information (ESI)

Electrochemical Nanoparticle-Enzyme Sensors for Screening Bacterial Contamination in Drinking Water

Juhong Chen,†[a] Ziwen Jiang,†[b] Jonathan D. Ackerman,[b] Mahdieh Yazdani,[b] Singyuk Hou,[b] Sam R. Nugen*[a] and Vincent M. Rotello*[b]

[a] *Department of Food Science, University of Massachusetts, 102 Holdsworth Way, Amherst, Massachusetts 01003, USA. E-mail: snugen@foodsci.umass.edu; Tel: +1-413-545-1262; Fax: +1-413-545-1025*

[b] *Department of Chemistry, University of Massachusetts, 710 North Pleasant Street, Amherst, Massachusetts 01003, USA. E-mail: rotello@chem.umass.edu; Tel.: +1-413-545-2058; Fax: +1-413-545-4490*

† These authors contributed equally to this work.

1. Optimization of Parameters for the Electrochemical Detection

After the *β*-galactosidase-catalyzed hydrolysis of PAPG, the cyclic voltammetry diagram of 4-aminophenol was obtained (**Fig. S1a**). The oxidation peak (E: 1.35 V) was between -0.1 and 0.4 V, which was selected as the range of differential pulse voltammetry (DPV) measurement. All electrochemical measurements were conducted using a portable Palmsens potentiostat. Parameters for the electrochemical measurement have been individually optimized. For equilibration time (t equilibration) before scanning, there was no significant difference from 0 to 5 second (**Fig. S1b**). A three-second equilibration time was used to allow -0.2 V (starting potential) to be applied at the working electrode before scanning. For step potential (E step), 5 mV was selected to collect data points and provided a better curve for comparison (**Fig. S1c**). Although the intensity of the electrochemical signal was enhanced at a higher pulse potential (E pulse), the peak shifting was observed (**Fig. S1d**). Pulse potential was set to 50 mV in order to increase the signal intensity and reduce the peak shift. The curve was improved at a higher pulse time (t pulse) setting (**Fig. S1e**). The highest pulse time which the instrument could achieve was 50 ms. No significant difference was observed among scan rates (**Fig. S1f**). However, experimental time could be reduced with a faster scan rate.

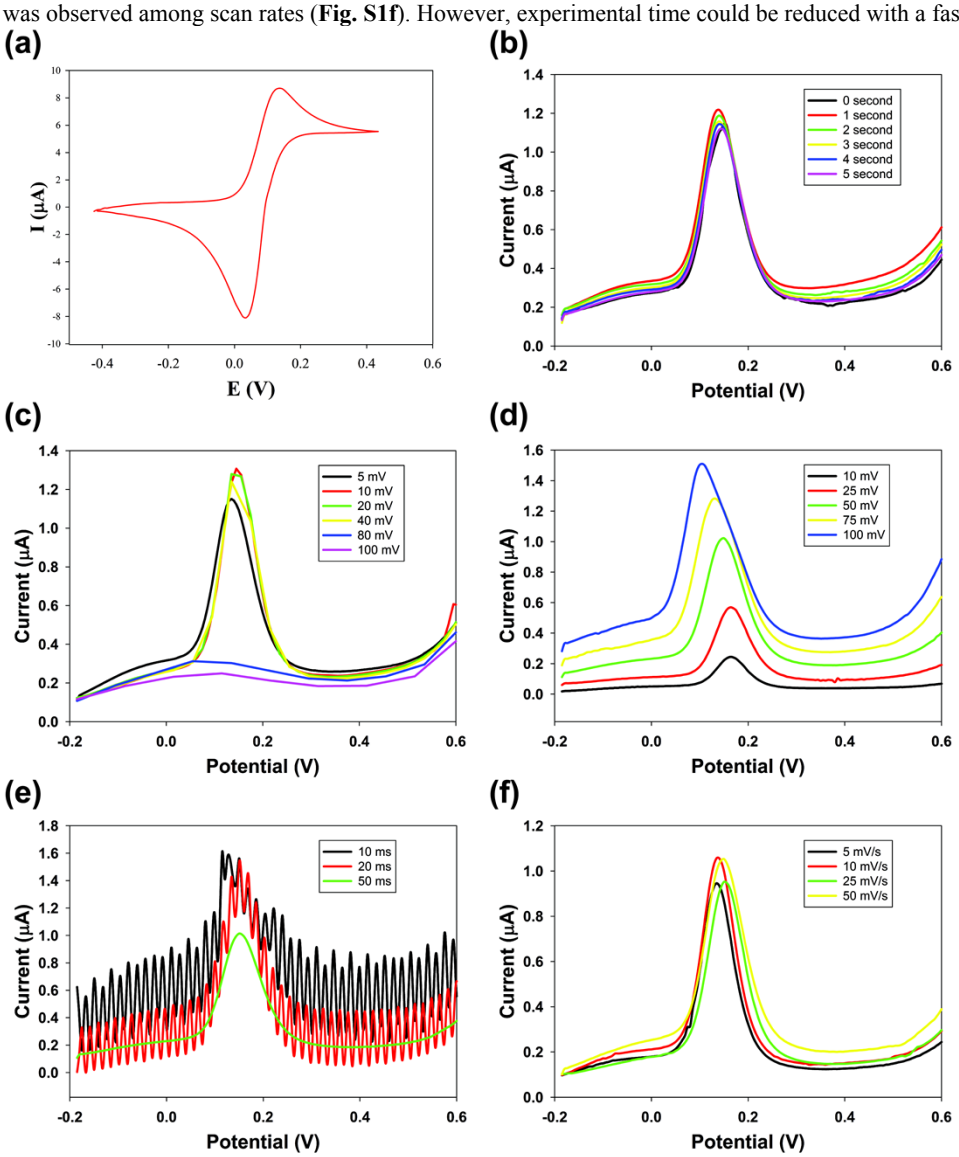

Fig. S1 (a) Cyclic voltammetry diagram of the mixture obtained after *β*-gal-catalyzed hydrolysis of PAPG. Optimization of the parameters for electrochemical detection (b) t equilibration, (c) E step, (d) E pulse, (e) t pulse and (f) scan rate.

2. Activity Titration for Gold Nanoparticles with Different Functionalization

We conducted the activity titration to investigate the inhibition behavior of **NP1**-**NP4** on *β*-gal, using *o*-nitrophenyl-*β*-galactopyranoside (ONPG) as a chromogenic substrate (**Fig. 2**). In this study, the *β*-gal was incubated with various concentrations of AuNPs for 30 minutes in PB buffer (5 mM pH 7.4). Samples without AuNPs were used for reference. With an increasing ratio of AuNPs to *β*-gal in the complex, the *β*-gal activity was suppressed until nearly complete inhibition was observed. The inhibition response for *β*-gal among different AuNPs was compared. The results demonstrated that **NP3** exhibited a stronger inhibition response for *β*-gal than the other ligands tested. The binding ratio for **NP3** in complex was 1.25, which enabled essentially complete inactivation of *β*-gal (**Fig. S2**).

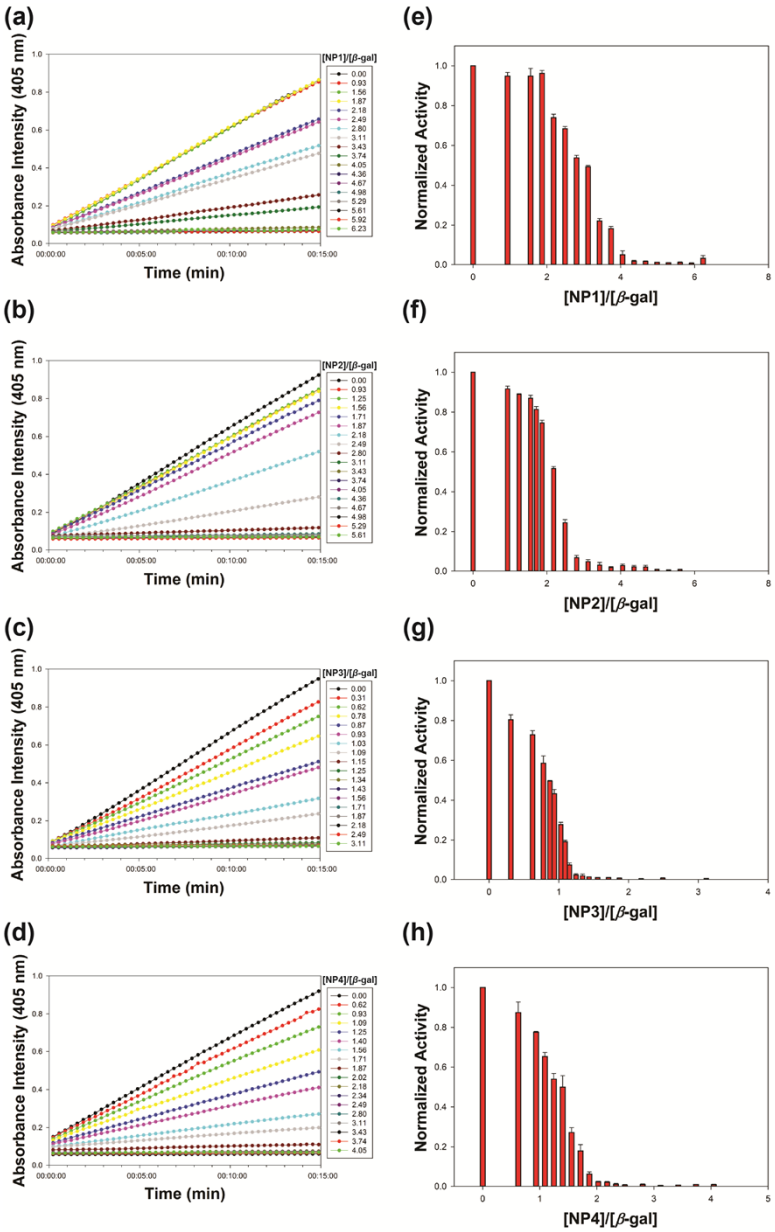

Fig. S2 Colorimetric activity inhibition of *β*-gal after incubation with different concentrations of (a) **NP1**, (b) **NP2**, (c) **NP3** and (d) **NP4**. Inhibited activity of *β*-gal plotted as cationic AuNPs concentrations in PB buffer (5 mM, pH 7.4). Optimal ratios of AuNPs/*β*-

gal complex (e) **NP1**: 4.36, (f) **NP2**: 3.43, (g) **NP3**: 1.25 and (h) **NP4**: 2.02. Error bars represent the standard deviation of a minimum of three replicates.

3. Calculations of Precision and Accuracy

Precision and accuracy were calculated using standard methods.[1] Having fifteen replicates (three replicates at five time points), precision of the analysis was calculated using coefficient of variation (CV):

$$\mathrm{CV} = \frac{s}{\overline{x}} \times 100\%$$

$$\%\ \mathrm{Precision} = 100 - \mathrm{CV}$$

where s is standard deviation and $\overline{x}$ is the average of the data (current value, I_p).

While precision is an estimate of random error, systematic error can be reported by calculating the accuracy of the analysis.[1] Accuracy was calculated according to the following formula:

$$\%\ \mathrm{Accuracy} = 100 \times \left(1 - \frac{|\mu - T|}{T}\right)$$

where μ is the mean of replicate measurements and T is the true value (spiked value) of analyte concentrations. A calibration curve was used to back calculate the concentrations (and then μ) from the instrumental signals.

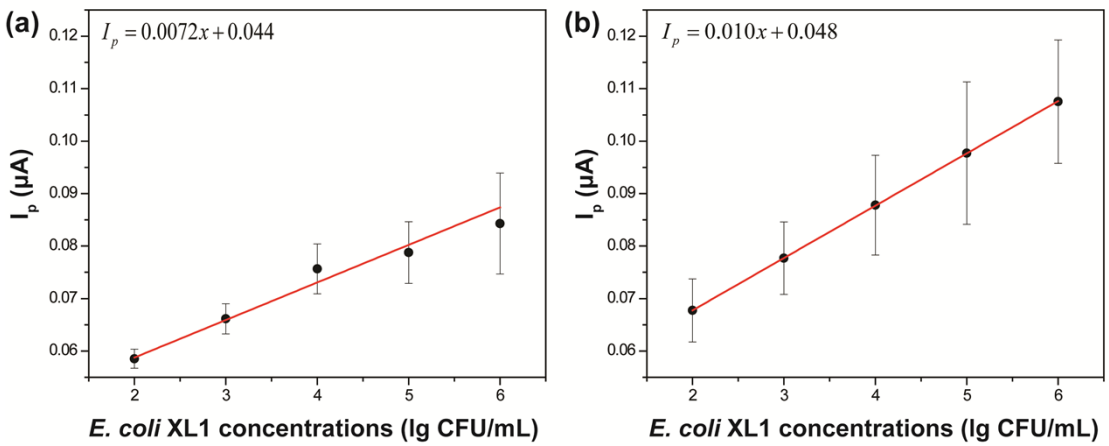

Fig. S3 Calibration curves for the sensor towards *E. coli* XL1 at (a) 16-minute incubation, (b) 28-minute incubation. In the linear fitting equations, *x* stands for the common logarithm of corresponding bacteria concentrations.

4. Relationship between Headgroup Hydrophobicity and the Corresponding Inhibition Efficiency of Enzyme Activity

The log *P* values of the ligand headgroups (**R_2** groups of **Fig. 2**) were estimated using ChemDraw Ultra 12.0 and reported in previous literatures.[2,3] Log *P* represents the calculated hydrophobic values of the headgroups. With the increase of the headgroup hydrophobicity [**NP1** (0.63) < **NP2** (3.65) < **NP4**: (3.77) < **NP3** (5.04)], the optimal ratios of AuNPs/*β*-gal complex for enzymatic activity inhibition (**Fig. S2**) decreased [**NP1** (4.36) > **NP2** (3.43) > **NP4** (2.02) > **NP3** (1.25)] (**Fig. S4**).

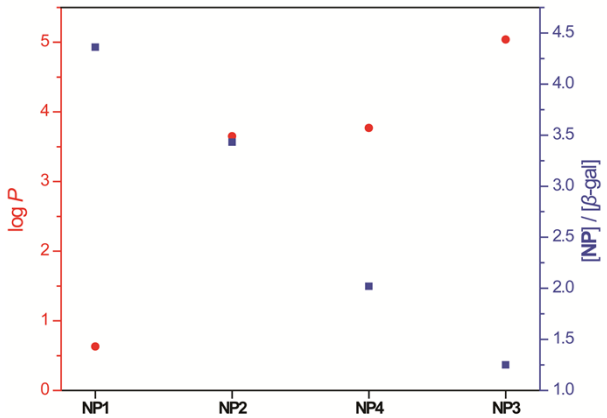

Fig. S4 Correlation of the calculated log *P* with the optimal ratio of AuNPs/*β*-gal complex for enzymatic activity inhibition.

5. Characterization of Gold Nanoparticles

5.1. Transmission Electron Microscope (TEM)

Transmission electron microscopy (TEM) was carried out on a JEOL 2000FX electron microscope. The core diameter of gold nanoparticles was analyzed by ImageJ (**Fig. S5**).[4]

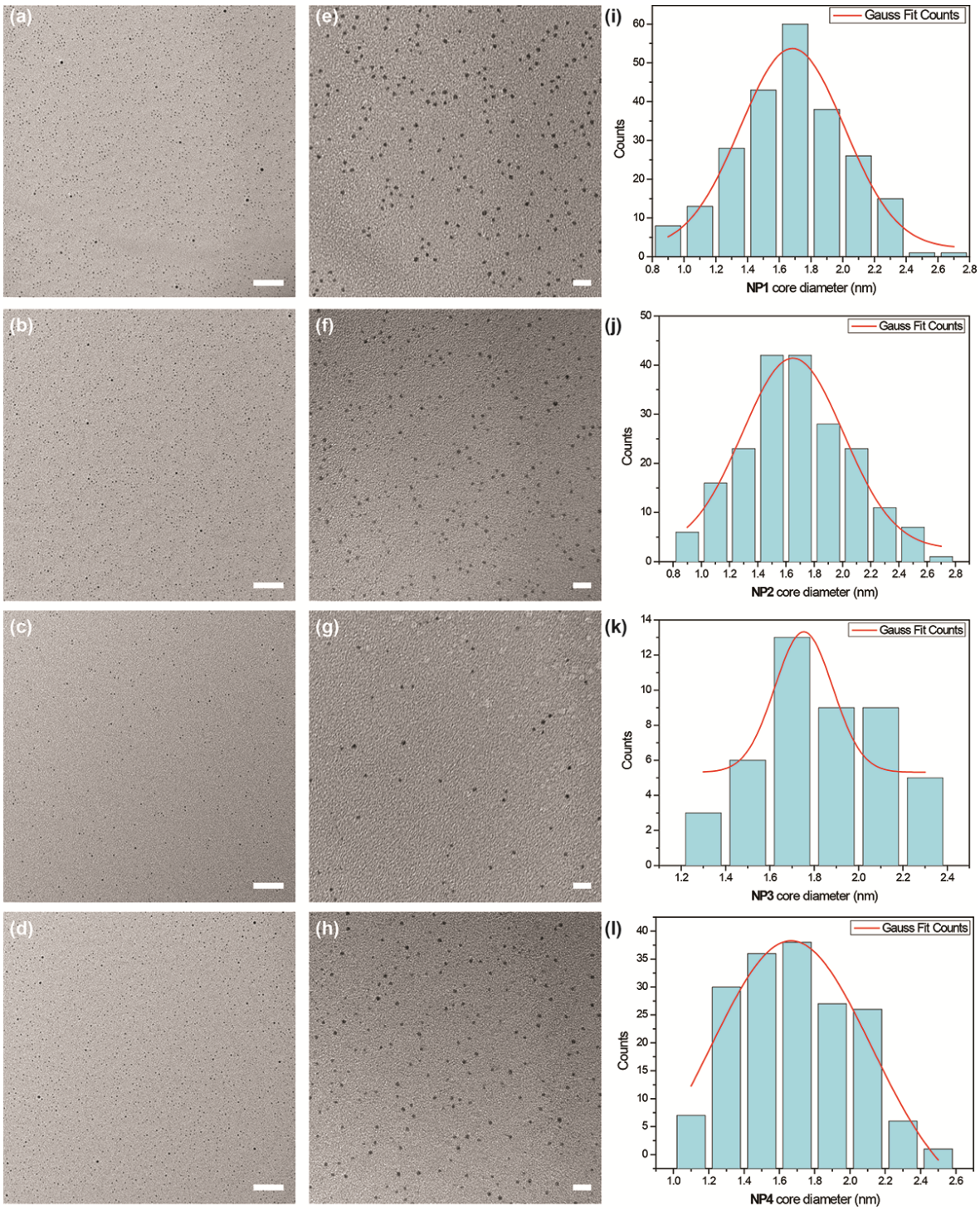

Fig. S5 (a) ~ (h) TEM images of **NP1-NP4**: (a), (e) **NP1**; (b), (f) **NP2**; (c), (g) **NP3**; (d), (h) **NP4**. The white scale bar is 50 nm in (a) ~ (d) and 10 nm in (e) ~ (h). (i) ~ (l) Core size distribution analysis for **NP1-NP4** corresponding to (e) ~ (h), respectively: (i) **NP1**: (1.7 ± 0.3) nm; (j) **NP2**: (1.6 ± 0.4) nm; (k) **NP3**: (1.8 ± 0.1) nm; (l) **NP4**: (1.7 ± 0.4) nm.

5.2. Dynamic Light Scattering (DLS) and Zeta Potential

Dynamic light scattering (DLS) profiles (**Fig. S6**) and zeta potential (**Fig. S7**) were recorded on a Malvern Zetasizer Nano ZS. The nanoparticles were diluted in sodium phosphate buffer (PB buffer, 5 mM, pH 7.4) to a concentration of 1 μM at room temperature.

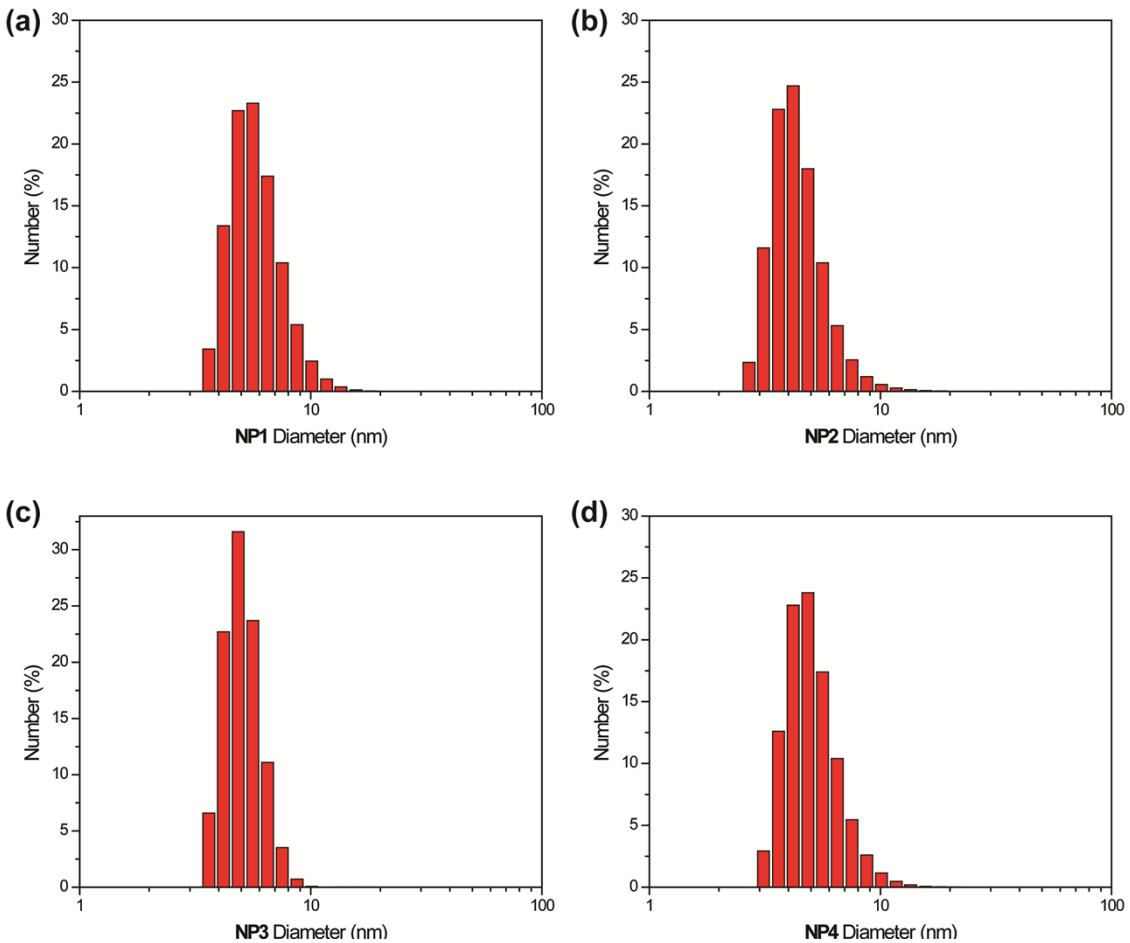

Fig. S6 DLS histogram of **NP1**-**NP4**, demonstrating the hydrodynamic diameter distribution of nanoparticles: (a) **NP1**, (b) **NP2**, (c) **NP3**, and (d) **NP4**.

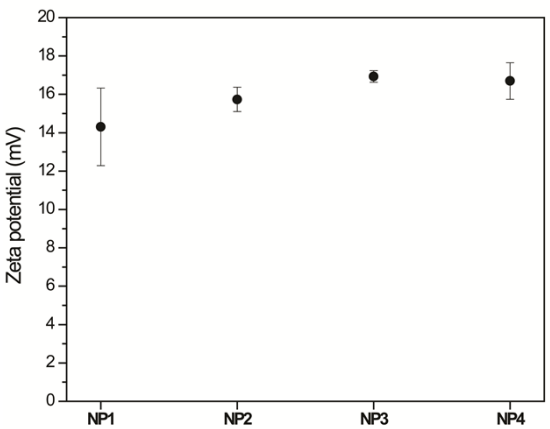

Fig. S7 Surface zeta potential of (a) **NP1**, (b) **NP2**, (c) **NP3**, and (d) **NP4**. Error bars represent the standard deviation of three replicates.

5.4. Laser Desorption Ionization Mass Spectrometry (LDI-MS)

LDI-MS measurements were carried out on a Bruker Autoflex III MALDI-TOF mass spectrometer (Bruker Daltonics, Germany) equipped with Smartbeam laser (Nd:YAG, 355 nm). All mass spectra were acquired in the reflectron mode and represent an average of 200 laser shots on each sample at a repetition frequency at 100 Hz under positive ionization mode. The ion source voltage 1 and 2 were set to 19.00 kV and 16.65 kV. The reflector voltage 1 and 2 were set to 21 kV and 9.7 kV. The laser power was set to be 60 % for each sample. The Bruker software (flexAnalysis version 3.3) was used for data analysis. LDI-MS results were used to confirm the monolayer composition of gold nanoparticles.

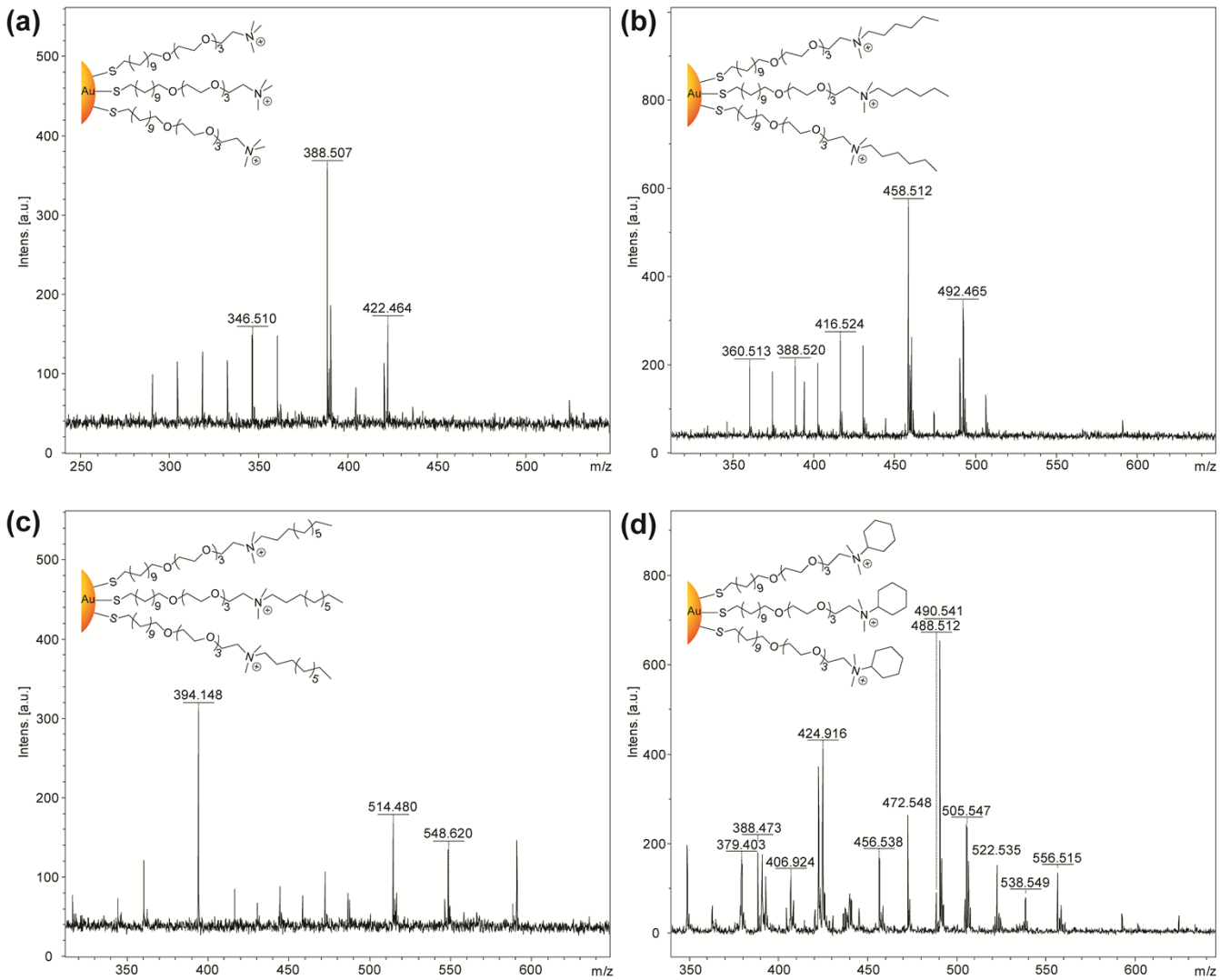

Fig. S8 LDI mass spectra of **NP1**-**NP4**: (a) **NP1**: MH^+ (*m/z* 422.5); (b) **NP2**: MH^+ (*m/z* 492.5); (c) **NP3**: MH^+ (*m/z* 548.6); (d) **NP4**: MH^+ (*m/z* 490.5). The LDI-MS results were consistent with previous reports.[5,6]

6. *Staphylococcus aureus* (*S. aureus*) detection

S. aureus CD-489[7] was cultured using similar procedures as *E. coli* XL1 (see "Experimental section" – "Bacterial culture" section). The electrochemical detection was also performed using similar procedures as *E. coli* XL1 (see "Experimental section" – "Analyte bacteria

response" section). The electrochemical detection results were shown in **Fig. S9** and the precision and accuracy calculations were shown in **Fig. S10**. The precision and accuracy of sensor operated at 16-minute incubation were calculated to be 88% and 87% respectively while the sensor operated at 28-minute incubation shows 88% precision and 86% accuracy.

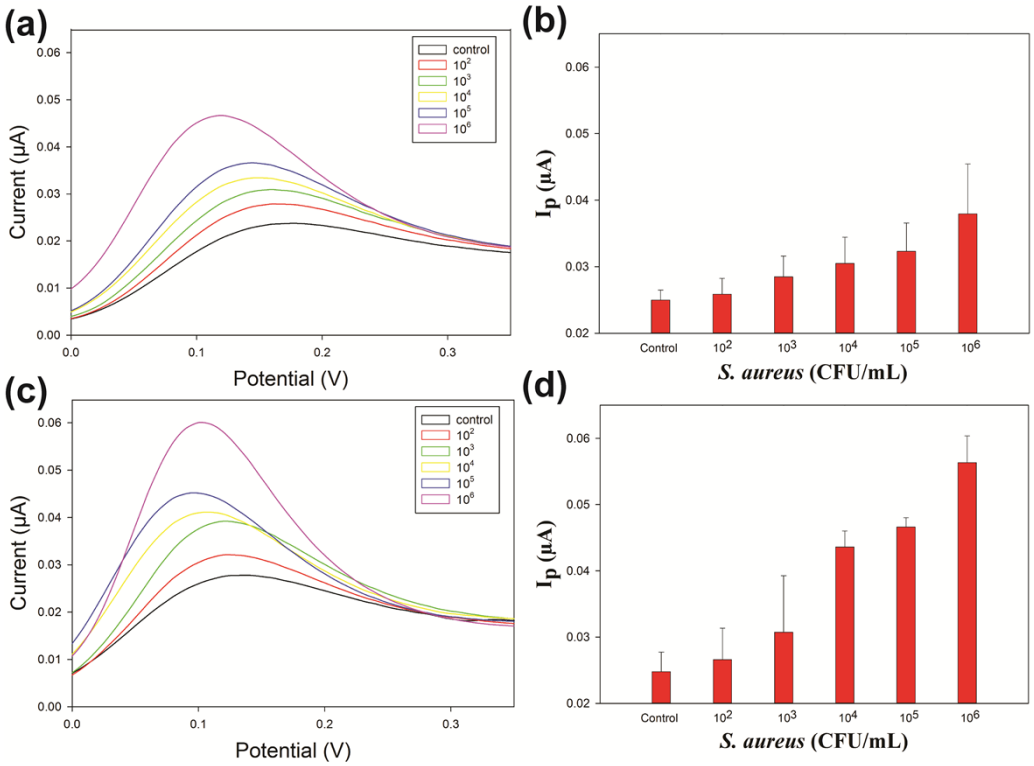

Fig. S9 Differential Pulse Voltammetry for the **NP3**/*β*-gal complex with increasing concentrations of *S. aureus* CD-489 (control, 1×10^2, 1×10^3, 1×10^4, 1×10^5 and 1×10^6 CFU·mL^{-1}) following incubation for (a) 16 minutes and (c) 28 minutes. Plot of numbers of *S. aureus* versus DPV signal after incubation for (b) 16 minutes and (d) 28 minutes. Error bars represent the standard deviation of a minimum of three replicates.

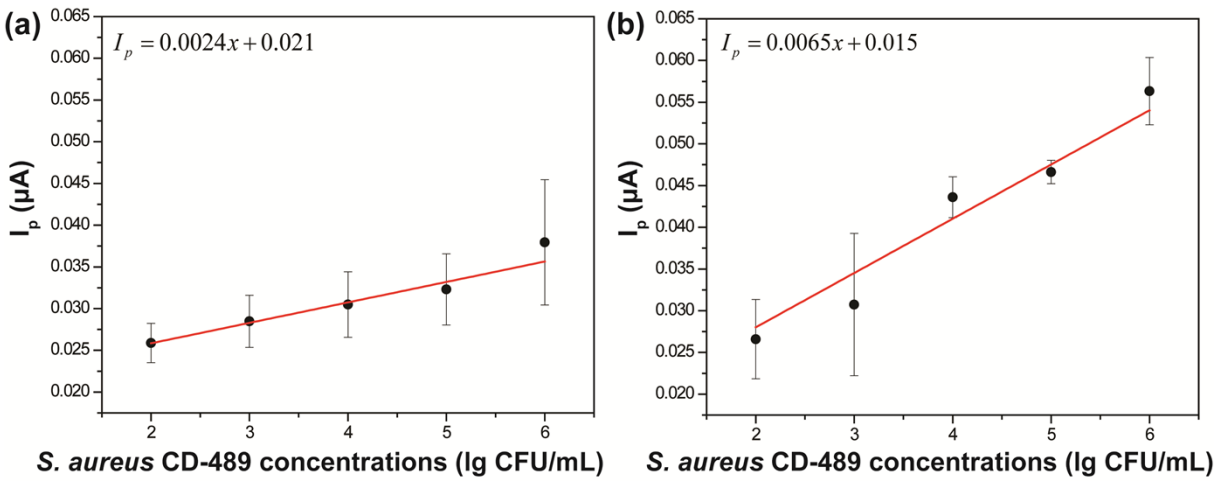

Fig. S10 Calibration curves for the sensor towards *S. aureus* CD-489 at (a) 16-minute incubation, (b) 28-minute incubation. In the linear fitting equations, *x* stands for the common logarithm of corresponding bacteria concentrations.

References

1. Skoog, D. A.; Holler, F. J.; Crouch, S. R., *Principles of Instrumental Analysis*. 6th Ed.; Thomson Brooks/Cole: Thomson Learning: USA, **2007**.

2. Moyano, D. F.; Goldsmith, M.; Solfiell, D. J.; Landesman-Milo, D.; Peer, D.; Rotello, V. M. "Nanoparticle Hydrophobicity Dictates Immune Response" *J. Am. Chem. Soc.* **2012**, *134*, 3965-3967.

3. Saha, K.; Moyano, D. F.; Rotello, V. M. "Protein Coronas Suppress the Hemolytic Activity of Hydrophilic and Hydrophobic Nanoparticles" *Mater. Horiz.* **2014**, *1*, 102-105.

4. Schneider, C.A.; Rasband, W.S.; Eliceiri, K.W. "NIH Image to ImageJ: 25 Years of Image Analysis" *Nat. Methods* **2012**, *9*, 671-675.

5. Zhu, Z.-J.; Ghosh, P.; Miranda, O. R.; Vachet, R. W.; Rotello, V. M. "Multiplexed Screening of Cellular Uptake of Gold Nanoparticles Using Laser Desorption/Ionization Mass Spectrometry" *J. Am. Chem. Soc.* **2008**, *130*, 14139-14143.

6. Yan, B.; Zhu, Z.-J.; Miranda O. R.; Chompoosor, A.; Rotello, V. M.; Vachet, R. W. "Laser Desorption/ionization Mass Spectrometry Analysis of Monolayer-protected Gold Nanoparticles" *Anal. Bioanal. Chem.* **2010**, *396*, 1025-1035.

7. Li, X.; Robinson, S. M.; Gupta, A.; Saha, K.; Jiang, Z.; Moyano, D. F.; Sahar, A.; Riley, M. A.; Rotello, V. M. "Functional Gold Nanoparticles as Potent Antimicrobial Agents against Multi-Drug-Resistant Bacteria" *ACS Nano* **2014**, *8*, 10682-10686.